ANALYTICAL SOLUTION FOR ROTATIONAL RUB-IMPACT PLATE UNDER THERMAL SHOCK

T.-Y. Zhao

School of Mechanical Engineering & Automation
Northeastern University
Shenyang, China

H.-Q. Yuan *

School of Science
Northeastern University
Shenyang, China

B.-B. Li

School of Mechanical Engineering & Automation
Northeastern University
Shenyang, China

Z.-J. Li

College of Resources and Civil Engineering
Northeastern University
Shenyang, China

L.-M. Liu

School of Science
Northeastern University
Shenyang, China

ABSTRACT

The analysis method is developed to obtain dynamic characteristics of the rotating cantilever plate with thermal shock and tip-rub. Based on the variational principle, equations of motion are derived considering the differences between rubbing forces in the width direction of the plate. The transverse deformation is decomposed into quasi-static deformation of the cantilever plate with thermal shock and dynamic deformation of the rubbing plate under thermal shock. Then deformations are obtained through the calculation of modal characteristics of rotating cantilever plate and temperature distribution function. Special attention is paid to the influence of tip-rub and thermal shock on the plate. The results show that tip-rub has the characteristics of multiple frequency vibrations, and high frequency vibrations are significant. On the contrary, thermal shock shows the low frequency vibrations. The thermal shock makes the rubbing plate gradually change into low frequency vibrations. Because rub-induced vibrations are more complicated than those caused by thermal shock, tip-rub is easier to result in the destruction of the blade. The increasing friction coefficient intensifies vibrations of the rubbing plate. Minimizing friction coefficients can be an effective way to reduce rub-induced damage through reducing the surface roughness between the blade tip and the inner surface of the casing.

Keywords: Rotating plate, Rubbing model, Thermal shock, Theoretical solution.

1. INTRODUCTION

Due to the fact that a small clearance in modern turbo machinery can cause serious rubbing malfunction for blades and the casing, rub-induced vibrations between rotating plates and stationary parts have drawn particular attention recently. Meanwhile, there are many such kinds of complicated dynamics in a contact-impact rotating plate. And a tip-rub blade from high-pressure compressor is often accompanied by the thermal shock problem. It will play an important role in engineering to research on the contact-impact characteristics of a rotating plate under thermal shock.

In the past, the majority of researches undertaken in this area have focused on disk models contacting with the casing. The first comprehensive review of the rubbing between the disks and stationary element was proposed by Muszynska [1]. Friction, impacting, stiffening and coupling effects were discussed. Choy and Padovan [2] investigated the problem of disks-casing rub interactions in rotating equipment. And the effects of casing stiffness, friction coefficient, as well as

* Corresponding author (yuanhq@mail.neu.edu.cn, 526356312@qq.com)

DOI : 10.1017/jmech.2016.19
Copyright © 2016 The Society of Theoretical and Applied Mechanics, R.O.C.
https://doi.org/10.1017/jmech.2016.19 Published online by Cambridge University Press

the interrelationship between rub force histories, energy levels, and rub duration were discussed.

In recent years, researchers study on structural contact problems by using more three-dimensional finite element numerical model [3,4]. Legrand *et al*. [5] proposed industrial finite element models to feature blade-tip/casing contact. The solution is computed with the augmented Lagrangian procedure. Batailly *et al*. [6] indicated that the large size of this finite element model would lead to extremely long computation times for explicit time integration simulations. In order to improve the computational efficiency, they used a component mode synthesis method to reduce the size of the model. In the case of contacts between blades of the rotor and the casing, the experimental phenomena were described in papers by Jiang *et al*. [7], Young [8], Garza [9], Ferguson [10] and Millecamps *et al*. [11]. Moreover, experimental results for a compressor blade rubbing a steel casing were obtained by Padova *et al*. [12,13]. The results describe the transient dynamics of the rotor and casing vibro-impact response at engine operational speeds similar to those experienced in flight.

In addition, several researchers have attempted to solve rubbing problems of rotating beams theoretically. Sinha [14,15] established the rotating beam system which was subjected to a periodic pulse load for local rubbing against the outer case. The periodic load was described by sine pulse wave, sine wave, and pulse distribution, respectively. And further consideration was given to the dynamic response of a rotating cantilever twisted Timoshenko beam subjected to contact loads at the free end. Lesaffre *et al*. [16,17] presented a model of Euler-Bernoulli beams clamped on the rigid disk to study the problem of contact between the flexible blades and the flexible casing. They also presented the stability analysis of a beam system rubbing on the ring. Neglecting shear deformation, Batailly *et al*. [18] established a rubbing model in which blade geometry and respective displacement field were discretized with the usual Euler-Bernoulli straight beam finite element.

Thermal transient analysis is very important when the blade have to undergo the change of temperature. And the theory to include the effect of thermal shock on plates has been paid more attention (*e.g.* see [19-23]). However, thermal effects on rub-induced vibrations of rotating plates have not received high concern due to the difficulties of theory analysis.

This study will thus develop a contact-impact model and present rub-induced theoretical vibration analysis of a rotating plate under thermal shock. Based on Hamilton principle, the equations of this system are derived considering the centrifugal stiffening effect. The analytical method is utilized to investigate dynamic responses of the rotating plate. And the present contact model is discussed when the plate impacts the casing. Then a series of discussions are carried out to assess the effects of the system parameters on the vibration characteristics of tip-rub. The characteristics of a rotating plate with tip-rub caused by thermal shock are especially investigated.

2. BASIC AND DYNAMIC EQUATIONS OF THE RUB-IMPACT MODEL

2.1 The Rub-Impact Model

The system to be analyzed, shown in Fig. 1, consists of a cantilevered rotating rectangular thin plate clamped at a rigid hub with radius R and constant rotation speed Ω. Since the hub is rigid, this model does not account for inter-blade coupling and one plate is investigated. The plate is characterized by length a, width b, thickness h and material properties Young's modulus E, mass per unit volume ρ and the Poisson ratio υ.

As indicated in Fig. 1, the plate is located in the inertia co-ordinate $OXYZ$ where X axis coincides with the horizontal direction, Y axis is parallel to generatrix of the hub and Z axis is along the plumb line. Flexible deformations of the plate are described in a local Cartesian coordinate system $OXYZ$. And it is fixed to the middle surface of the plate rotating and moving relative to the inertia co-ordinate $OXYZ$. The x-axis and y-axis are the in-plane coordinates and z is an axis perpendicular to its surface. The plate undergoes a sudden constant thermal flow q_T on their surface. And they are exposed to a sudden temperature rise, which leads to thermal vibration. Small deformations of each point in the middle surface of the plate are only denoted as w along the z direction. Rub-impact loads at the free end are applied to the plate, including the impact load F_a and the friction force between the casing and this plate μF_a. They are nonzero only when the tip travelling through the rub zone on the casing. It should be noted that the rubbing position may be any line segment at the free end. The rotary inertia effects of this thin plate are ignored in this study.

2.2 Differential Equations of Motion

Since an energetic method is used to develop this model, the kinetic energy T_p can be fully expressed by the following relation

$$T_\mathrm{p} = \frac{1}{2}\rho h\int_0^b\int_0^a\left[w^2\Omega^2+\left(\frac{\partial w}{\partial t}\right)^2+(R+x)^2\Omega^2-2\frac{\partial w}{\partial t}(R+x)\Omega\right]\mathrm{d}x\mathrm{d}y \tag{1}$$

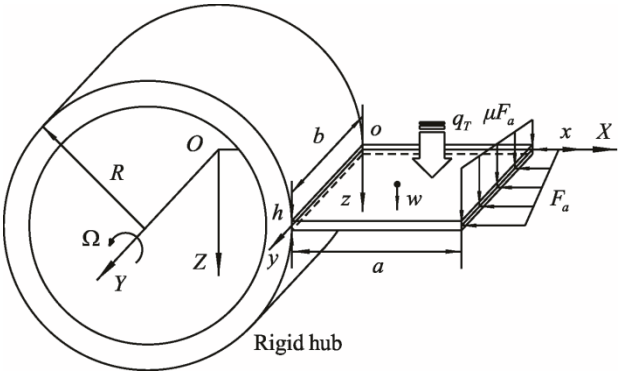


Fig. 1 The rub-impact model of a rotating plate under thermal shock.

https://doi.org/10.1017/jmech.2016.19 Published online by Cambridge University Press

It is assumed that the change of temperature $T_h(x, y, z, t)$ does not affect the mechanical properties and thermal properties of materials. The relations between the stress and strain components including the thermal effect are obtained

$$\begin{cases} \sigma_x = \dfrac{E}{1-\upsilon^2}\left[(\varepsilon_x + \upsilon\varepsilon_y) - (1+\upsilon)a_T T_h\right] \\ \sigma_y = \dfrac{E}{1-\upsilon^2}\left[(\varepsilon_y + \upsilon\varepsilon_x) - (1+\upsilon)a_T T_h\right] \\ \tau_{xy} = G\gamma_{xy} \end{cases} \tag{2}$$

where a_T is the material's coefficient of thermal expansion. The micro-elastic strain energy $\mathrm{d}U_1$ can be expressed as follows considering the thermal effect

$$\begin{aligned} \mathrm{d}U_1 &= \frac{1}{2}\left[\sigma_x(\varepsilon_x - a_T T) + \sigma_y(\varepsilon_y - a_T T) + \tau_{xy}\gamma_{xy}\right] \\ &= \frac{1}{2}\left[\begin{array}{l} \dfrac{E}{1-\upsilon^2}\left[(\varepsilon_x + \upsilon\varepsilon_y)\varepsilon_x + (\varepsilon_y + \upsilon\varepsilon_x)\varepsilon_y\right] \\ +G\gamma_{xy}\gamma_{xy} + \dfrac{E}{1-\upsilon^2}2(1+\upsilon)(a_T T)^2 \\ +\dfrac{E}{1-\upsilon^2}\left[-2(1+\upsilon)a_T T\varepsilon_x - 2(1+\upsilon)\,a_T T\varepsilon_y\right] \end{array}\right] \end{aligned} \tag{3}$$

Bending strains ε_x, ε_y, ε_{xy} are related to transverse deformation w by the following three relations

$$\varepsilon_x = -\frac{\partial^2 w}{\partial x^2}z\,,\quad \varepsilon_y = -\frac{\partial^2 w}{\partial y^2}z\,,\quad \gamma_{xy} = -2\frac{\partial^2 w}{\partial x \partial y}z \tag{4}$$

Substituting Eqs. (2), (4) into Eq. (3), the energy of bending is obtained. It can be written as follows through integral

$$U_1 = \frac{D}{2}\int_0^b\int_0^a \left[\begin{array}{l} \left(\dfrac{\partial^2 w}{\partial x^2}\right)^2 + \left(\dfrac{\partial^2 w}{\partial y^2}\right)^2 + 2\upsilon\left(\dfrac{\partial^2 w}{\partial x^2}\right)\left(\dfrac{\partial^2 w}{\partial y^2}\right) \\ +2(1-\upsilon)\left(\dfrac{\partial^2 w}{\partial x \partial y}\right)^2 \\ +2(1+\upsilon)\,a_T M_T\left(\dfrac{\partial^2 w}{\partial x^2}\right) \\ +2(1+\upsilon)\,a_T M_T\left(\dfrac{\partial^2 w}{\partial y^2}\right) \end{array}\right] \mathrm{d}x\mathrm{d}y \tag{5}$$

where a_T is thermal expansion coefficient. Flexural rigidity of the plate D is equal to $Eh^3/12(1-\upsilon^2)$. Thermal bending moment M_T is $M_T(x, y, t) = \dfrac{12}{h^3}\int_{-h/2}^{h/2} T_h(x, y, z, t)\, z\mathrm{d}z$. T_h is temperature distribution function on the plate. And the rotation-induced centrifugal potential energy U_2 can be expressed as

$$U_2 = \frac{1}{2}\rho h\Omega^2\int_0^b\int_0^a\left\{\left[R(a-x) + \frac{1}{2}(a^2 - x^2)\right]\left(\frac{\partial w}{\partial x}\right)^2\right\}\mathrm{d}x\mathrm{d}y \tag{6}$$

Then the total strain energy of the plate is obtained, and are defined as

$$U = U_1 + U_2 \tag{7}$$

In general, the wave-form of the periodic rub loads can have many different time-dependent distributions. Based on the experiment results [15,16], sine pulse loading at the free-end has been observed for tip-rub. Moreover, Sinha [1,2] showed that a continuous sine function of the time t may be valid in some special situations, such as when the spin velocity Ω is very high or, the rub-zone is circumferentially so large that it is fair to assume almost a 360° rub on the stator. Therefore, in this paper, two kinds of functions are introduced including sine wave and sine pulse wave which are the main forms in tip-rub. Especially for the plate model, rub loads are a function of the in-plane coordinate y. Firstly, the following periodic pulse loading with the form of Fourier series has been used (see Fig. 2(a)).

$$F_a(y, t) = a_0 + \sum_{k=1}^{\infty}\left(a_k\cos\frac{2k\pi}{T}t + b_k\sin\frac{2k\pi}{T}t\right) \tag{8}$$

where

$$\begin{aligned} a_0 &= \frac{1}{T}\int_0^{t_p}\left[F_{\max}\sin(\pi t/t_p)\right]\mathrm{d}t,\ a_k \\ &= \frac{2}{T}\int_0^{t_p}\left[F_{\max}\sin(\pi t/t_p)\cos(2k\pi t/T)\right]\mathrm{d}t \\ b_k &= \frac{2}{T}\int_0^{t_p}\left[F_{\max}\sin(\pi t/t_p)\sin(2k\pi t/T)\right]\mathrm{d}t \end{aligned} \tag{9}$$

where t_p is the contact load time, and T is the period of rub loads. Furthermore, $F_{\max}$ is the excitation amplitude at the tip, which is a function of rub position given by $F_{\max}(y)$.

Secondly, a continuous sine function of time t is used as the rub load which can be expressed as (see Fig. 2(b))

$$F_a(y, t) = F_{\max}(y)\cdot\left[1 - \cos(\omega t)\right] \tag{10}$$

where ω is angular frequency of the rub load. Moreover, $F_a(y, t)$ can be rewritten as follows in Eqs. (11) and (12).

$$F_a(y, t) = F_{\max}(y)\cdot F(t) \tag{11}$$

Actually, the excitation amplitude $F_{\max}$ has the following forms as shown in Fig. 3.

$$F_{\max}(y) = \frac{F_2 - F_1}{b}y + F_1 \tag{12}$$

where F_1 and F_2 are the maximum and minimum rub load, respectively.

https://doi.org/10.1017/jmech.2016.19 Published online by Cambridge University Press

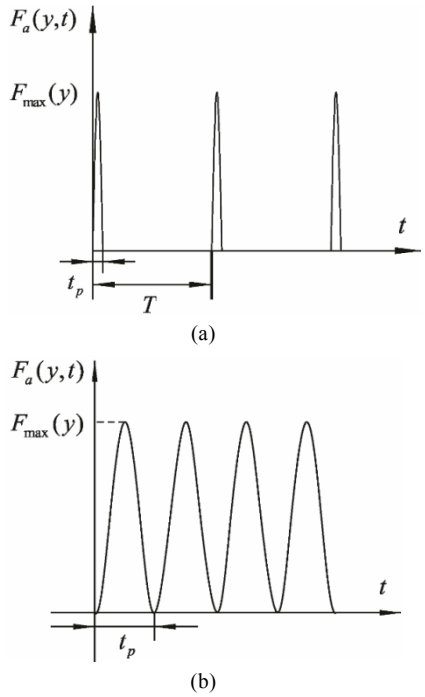


Fig. 2 The time history curve of axial rub load given by Eq. (8).

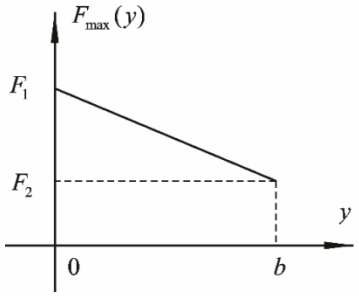


Fig. 3 The relation between rub load amplitude and width coordinate.

Then the virtual work δW done by the rub loads is written as

$$\delta W_P = q(x, y, t)\,\delta w \tag{13}$$

where, $q(x, y, t) = \mu F_a(t)\,\delta(x-\xi)\,\delta(y-\eta)$ or $q(x, y, t) = \mu F_a(y, t)\,\delta(x-\xi)$.

The Hamilton principle gives the equation

$$\delta\int_{t_0}^{t_1}(T_p - U)\,\mathrm{d}t + \int_{t_0}^{t_1}\int_0^a\int_0^b \delta W\,\mathrm{d}x\mathrm{d}y\mathrm{d}t = 0 \tag{14}$$

By substituting Eqs. (1), (7), (13) into Eq. (14), variational equations are given by

$$\begin{aligned}
&\int_0^b\int_0^a\Bigg\{\rho h w\Omega^2 - \rho h\ddot{w} - D\left[\frac{\partial^4 w}{\partial x^4} + 2\frac{\partial^4 w}{\partial x^2\partial y^2} + \frac{\partial^4 w}{\partial y^4}\right]\\
&+\rho h\Omega^2\left[R(a-x) + \frac{1}{2}(a^2 - x^2)\right]\frac{\partial^2 w}{\partial x^2} - \rho h\Omega^2(R+x)\frac{\partial w}{\partial x}\\
&-D(1+\upsilon)a_T\frac{\partial^2 M_T}{\partial x^2} - D(1+\upsilon)a_T\frac{\partial^2 M_T}{\partial y^2}\Bigg\}\mathrm{d}x\mathrm{d}y\\
&= \int_0^b\int_0^a -q(x, y, t)\,\mathrm{d}x\mathrm{d}y
\end{aligned} \tag{15}$$

After simplification, Eq. (15) is expressed as

$$\begin{aligned}
&\rho h w\Omega^2 - \rho h\ddot{w} - D\left[\frac{\partial^4 w}{\partial x^4} + 2\frac{\partial^4 w}{\partial x^2\partial y^2} + \frac{\partial^4 w}{\partial y^4}\right]\\
&+\rho h\Omega^2\left[R(a-x) + \frac{1}{2}(a^2 - x^2)\right]\frac{\partial^2 w}{\partial x^2}\\
&-\rho h\Omega^2(R+x)\frac{\partial w}{\partial x} - D(1+\upsilon)\,a_T\frac{\partial^2 M_T}{\partial x^2}\\
&-D(1+\upsilon)\,a_T\frac{\partial^2 M_T}{\partial y^2} = -q(x, y, t)
\end{aligned} \tag{16}$$

Because the temperature distribution of space and time process is known, nonhomogeneous items on the right side of the equation act as known functions. It is the equivalent of load items. The problem turns to a forced vibration one. Then the solution of differential equation can be written as a sum of two parts

$$w = w_s + w_m \tag{17}$$

where w_s is the quasi-static solution of cantilever plate under thermal shock, w_m is the dynamic solution of rub-impact plate under thermal shock. They are shown as the following expressions

$$\nabla^2\nabla^2 w_s + (1+\upsilon)\,a_T\nabla^2 M_T = 0 \tag{18}$$

$$\begin{aligned}
&\rho h(\ddot{w}_m + \ddot{w}_s) + D\left[\frac{\partial^4 w_m}{\partial x^4} + 2\frac{\partial^4 w_m}{\partial x^2\partial y^2} + \frac{\partial^4 w_m}{\partial y^4}\right]\\
&+\rho h\Omega^2(R+x)\frac{\partial(w_m + w_s)}{\partial x}\\
&-\rho h\Omega^2\left[R(a-x) + \frac{1}{2}(a^2 - x^2)\right]\frac{\partial^2(w_m + w_s)}{\partial x^2}\\
&-\rho h(w_m + w_s)\,\Omega^2 = q(x, y, t)
\end{aligned}$$

Namely

$$\begin{aligned}
&\rho h\ddot{w}_m + D\left[\frac{\partial^4 w_m}{\partial x^4} + 2\frac{\partial^4 w_m}{\partial x^2\partial y^2} + \frac{\partial^4 w_m}{\partial y^4}\right]\\
&-\rho h\Omega^2\left[R(a-x) + \frac{1}{2}(a^2 - x^2)\right]\frac{\partial^2 w_m}{\partial x^2}\\
&-\rho h w_m\Omega^2 + \rho h\Omega^2(R+x)\frac{\partial w_m}{\partial x} = q(x, y, t) + \rho h w_s\Omega^2 - \rho h\ddot{w}_s\\
&-\rho h\Omega^2(R+x)\frac{\partial w_s}{\partial x} + \rho h\Omega^2\left[R(a-x) + \frac{1}{2}(a^2 - x^2)\right]\frac{\partial^2 w_s}{\partial x^2}
\end{aligned} \tag{19}$$

https://doi.org/10.1017/jmech.2016.19 Published online by Cambridge University Press

Equation (18) is for the quasi-static problem and can be solved by the cantilever plate static problem solution. Then substituting w_s into Eq. (19), the dynamic solution is obtained.

3. ANALYTICAL SOLUTION FOR RUB-IMPACT PLATE UNDER THERMAL SHOCK

3.1 The Modal Characteristics of Rotating Plate

The deformation w which satisfy geometrical boundary condition of the plate is expanded by using the following expression

$$w(x, y, t) = W(x, y)\sin(\omega t + \phi) \tag{20}$$

where

$$W(x, y) = \sum_{m=1}^{M}\sum_{n=1}^{N} A_{mn}\,\phi_m(x)\,\varphi_n(y) \tag{21}$$

where m and n are the numbers of waves in x-and y-direction respectively. $A_{mn}(t)$ is the generalized coordinate and the unknown functions of the time t. M and N are the numbers of necessary terms in the expansions of the in-plane deformations. Cantilever beam mode function $\phi_m(x)$ and free-free beam mode function $\varphi_n(y)$ can be obtained by

$$\begin{aligned}\phi_m(x) &= \cosh(\alpha_m x) - \cos(\alpha_m x) \\ &\quad - \frac{\cos(\alpha_m a) + \cosh(\alpha_m a)}{\sin(\alpha_m a) + \sinh(\alpha_m a)}\left[\sinh(\alpha_m x) - \sin(\alpha_m x)\right] \\ \varphi_n(y) &= \cosh(\beta_n y) + \cos(\beta_n y) \\ &\quad - \frac{\cos(\beta_n b) - \cosh(\beta_n b)}{\sin(\beta_n b) - \sinh(\beta_n b)}\left[\sinh(\beta_n y) + \sin(\beta_n y)\right]\end{aligned} \tag{22}$$

where α_m, β_n are determined by

$$\cosh(\alpha_m a)\cos(\alpha_m a) + 1 = 0,\ \ \cosh(\beta_n b)\cos(\beta_n b) - 1 = 0 \tag{23}$$

Equation (20) which contains $M \times N$ parameters is substituted into the Hamiltonian equation with no virtual work item. It can be simplified as follows through integral of a cycle

$$\int_0^b\int_0^a \left\{\begin{aligned}&\rho h(\omega^2+\Omega^2)W\delta W - \frac{1}{2}\rho h\Omega^2(a^2-x^2)\frac{\partial W}{\partial x}\delta\left(\frac{\partial W}{\partial x}\right) \\ &-D\left[\begin{aligned}&\left(\frac{\partial^2 W}{\partial x^2}\right)\delta\left(\frac{\partial^2 W}{\partial x^2}\right)+\left(\frac{\partial^2 W}{\partial y^2}\right)\delta\frac{\partial^2 W}{\partial y^2} \\ &+\frac{\partial^2 W}{\partial x^2}\delta\left(\frac{\partial^2 W}{\partial y^2}\right)+\frac{\partial^2 W}{\partial y^2}\delta\left(\frac{\partial^2 W}{\partial x^2}\right)\end{aligned}\right] \\ &+D(1-\upsilon)\left[\frac{\partial^2 W}{\partial x^2}\delta\left(\frac{\partial^2 W}{\partial y^2}\right)+\frac{\partial^2 W}{\partial y^2}\delta\left(\frac{\partial^2 W}{\partial x^2}\right)-2\frac{\partial^2 W}{\partial x\partial y}\delta\left(\frac{\partial^2 W}{\partial x\partial y}\right)\right]\end{aligned}\right\}\mathrm{d}x\mathrm{d}y = 0 \tag{24}$$

Substituting Eq. (21) into Eq. (24) and generate the variational coefficient A_{mn}. Making the coefficient of δA_{mn} to be zero, we can get $M \times N$ homogeneous equations. Because coefficient determinant of the equations must be zero, the frequency equation is obtained as follows

$$\int_0^b\int_0^a \left\{\begin{aligned}&D(1-\mu)\left[-2\sum_{m=1}^{M}\sum_{n=1}^{N} A_{mn}\varphi_m'(x)\,\varphi_n'(y)\,\phi_i'(x)\,\varphi_j'(y)\right] \\ &-\mu D\left[\begin{aligned}&\sum_{m=1}^{M}\sum_{n=1}^{N} A_{mn}\,\varphi_m''(x)\,\varphi_n(y)\,\phi_i(x)\varphi_j''(y) \\ &+\sum_{m=1}^{M}\sum_{n=1}^{N} A_{mn}\,\varphi_m(x)\varphi_n''(y)\,\phi_i(x)''\varphi_j(y)\end{aligned}\right] \\ &+\rho h(\omega^2+\Omega^2)\sum_{m=1}^{M}\sum_{n=1}^{N} A_{mn}\varphi_m(x)\,\varphi_n(y)\,\phi_i(x)\,\varphi_j(y) \\ &-D\left[\begin{aligned}&\sum_{m=1}^{M}\sum_{n=1}^{N} A_{mn}\,\varphi_m''(x)\,\varphi_n(y)\,\phi_i(x)''\varphi_j(y) \\ &+\sum_{m=1}^{M}\sum_{n=1}^{N} A_{mn}\,\varphi_m(x)\varphi_n''(y)\,\phi_i(x)\,\varphi_j''(y)\end{aligned}\right] \\ &-\frac{1}{2}\rho h\Omega^2(a^2-x^2)\sum_{m=1}^{M}\sum_{n=1}^{N} A_{mn}\,\varphi_m'(x)\,\varphi_n(y)\varphi_i'(x)\,\varphi_j(y)\end{aligned}\right\}\mathrm{d}x\mathrm{d}y = 0 \tag{25}$$

https://doi.org/10.1017/jmech.2016.19 Published online by Cambridge University Press

Equation (25) can be expressed simply for further

$$\rho h(\omega^2+\Omega^2)\hat{\boldsymbol{E}}-D\upsilon(\hat{\boldsymbol{H}}+\hat{\boldsymbol{G}}-2\hat{\boldsymbol{K}})-D(\hat{\boldsymbol{I}}+\hat{\boldsymbol{F}}+2\hat{\boldsymbol{K}})-\rho h\Omega^2\hat{\boldsymbol{L}}=0 \tag{26}$$

where the elements of the (i, j) line of the (m, n) column of $\hat{\boldsymbol{E}}$、$\hat{\boldsymbol{F}}$、$\hat{\boldsymbol{G}}$、$\hat{\boldsymbol{H}}$、$\hat{\boldsymbol{I}}$、$\hat{\boldsymbol{K}}$、$\hat{\boldsymbol{L}}$ are E_{mn}^{ij}、F_{mn}^{ij}、G_{mn}^{ij}、H_{mn}^{ij}、I_{mn}^{ij}、K_{mn}^{ij}、L_{mn}^{ij}, respectively. They have the following forms.

$$\begin{cases}
E_{mn}^{ij}=\int_0^b\int_0^a \phi_m(x)\,\varphi_n(y)\,\phi_i(x)\,\varphi_j(y)\,\mathrm{d}x\mathrm{d}y\\
F_{mn}^{ij}=\int_0^b\int_0^a \phi_m''(x)\,\varphi_n(y)\,\phi_i''(x)\,\varphi_j(y)\,\mathrm{d}x\mathrm{d}y\\
G_{mn}^{ij}=\int_0^b\int_0^a \phi_m(x)\,\varphi_n''(y)\,\phi_i''(x)\,\varphi_j(y)\,\mathrm{d}x\mathrm{d}y\\
H_{mn}^{ij}=\int_0^b\int_0^a \phi_m''(x)\,\varphi_n(y)\,\phi_i(x)\,\varphi_j''(y)\,\mathrm{d}x\mathrm{d}y\\
I_{mn}^{ij}=\int_0^b\int_0^a \phi_m(x)\,\varphi_n''(y)\,\phi_i(x)\,\varphi_j''(y)\,\mathrm{d}x\mathrm{d}y\\
K_{mn}^{ij}=\int_0^b\int_0^a \phi_m'(x)\,\varphi_n'(y)\,\phi_i'(x)\,\varphi_j'(y)\,\mathrm{d}x\mathrm{d}y\\
L_{mn}^{ij}=\int_0^b\int_0^a \left[R(a-x)+\frac{1}{2}(a^2-x^2)\right]\phi_m'(x)\,\varphi_n(y)\,\phi_i'(x)\,\varphi_j(y)\,\mathrm{d}x\mathrm{d}y
\end{cases} \tag{27}$$

Each order natural frequency values ω_{mn} and the corresponding vibration modes W_{mn} can be calculated based on the frequency equation above.

3.2 Analytical Solution for Temperature Distribution Function

The temperature field T_h under consideration is reduced to one-dimensional thermal conduction problem and is governed by

$$\lambda\frac{\partial^2 T_h}{\partial z^2}=C\rho\frac{\partial T_h}{\partial t} \tag{28}$$

where λ is the coefficient of thermal conductivity, C is specific heat, and ρ is the density. The following initial and boundary conditions are considered

$$t=0,\quad T=0 \tag{29}$$

$$z=\frac{h}{2},\ \lambda\frac{\partial T_h}{\partial z}=q_T\ ;\ z=-\frac{h}{2},\ \frac{\partial T_h}{\partial z}=0 \tag{30}$$

And the temperature field is given by the solution

$$T_h(z,t)=\frac{q_T h}{\lambda}\left[\frac{\beta t}{\pi^2}+\frac{3z^2+3hz-\frac{h^2}{4}}{6h^2}-\frac{2}{\pi^2}\sum_{n=1}^{\infty}\frac{(-1)^n}{n^2}e^{-n^2\beta t}\cos\frac{n\pi}{2}\left(\frac{2z}{h}+1\right)\right],\quad \beta=\frac{\lambda\pi^2}{C\rho h^2} \tag{31}$$

Based on $\int_{-h/2}^{h/2} z\cos\frac{n\pi}{2}\left(\frac{2z}{h}+1\right)\mathrm{d}z=-\sum_{n=1,3,5,\infty}\frac{2h^2}{n^2\pi^2}$, the thermal bending moment M_T have the following form

$$M_T(t)=\frac{q_T}{2\lambda}\left\{1-\frac{96}{\pi^4}\sum_{n=1,3,5}^{\infty}\frac{e^{-n^2\beta t}}{n^4}\right\} \tag{32}$$

3.3 Quasi-Static Solution for Cantilever Plate Under Thermal Shock

Equation (18) which is the quasi-static equation of cantilever plate under thermal shock can be solved by the Ritz method. Bending deformation potential energy of cantilever rectangular plate can be express as

https://doi.org/10.1017/jmech.2016.19 Published online by Cambridge University Press

$$U_T = \frac{D}{2}\int_0^b\int_0^a\left\{\left(\frac{\partial^2 w_s}{\partial x^2}\right)^2+\left(\frac{\partial^2 w_s}{\partial y^2}\right)^2+2\upsilon\left(\frac{\partial^2 w_s}{\partial x^2}\right)\left(\frac{\partial^2 w_s}{\partial y^2}\right)+2(1-\upsilon)\left(\frac{\partial^2 w_s}{\partial x\partial y}\right)^2\right\}\mathrm{d}x\mathrm{d}y \tag{33}$$

The deformations w_s is expanded by using the expression $w_s = \sum_{m=1}^{M}\sum_{n=1}^{N} B_{mn}\,\phi_m(x)\,\varphi_n(y)$. Then the equation of the variable B_{ij} can be obtained as follows

$$\frac{\partial U_T}{\partial B_{ij}} = \int_0^b\int_0^a -D(1+\upsilon)\,a_T[\nabla^2 M_T]\,\phi_i(x)\,\varphi_j(y)\,\mathrm{d}x\mathrm{d}y \tag{34}$$

The thermal bending moment can be expressed as trigonometric series

$$M_T = \frac{1}{2\lambda}\left\{1-\frac{96}{\pi^4}\sum_{n=1,3,5}^{\infty}\frac{e^{-n^2\beta t}}{n^4}\right\}\sum_{m=1}^{\infty}\sum_{n=1}^{\infty}\frac{4q_T}{\pi^2 mn}(1-\cos m\pi)(1-\cos n\pi)\sin\frac{m\pi x}{a}\sin\frac{n\pi y}{b} \tag{35}$$

So the right side of Eq. (34) can be simplified as follows

$$\begin{aligned} &D(1+\upsilon)\,a_T\,\frac{1}{2\lambda}\left\{1-\frac{96}{\pi^4}\sum_{n=1,3,5}^{\infty}\frac{e^{-n^2\beta t}}{n^4}\right\} \\ &\cdot\sum_{m=1}^{\infty}\sum_{n=1}^{\infty}\left\{\frac{4q_T}{\pi^2 mn}(1-\cos m\pi)(1-\cos n\pi)\cdot\left[\left(\frac{m\pi}{a}\right)^2+\left(\frac{n\pi}{b}\right)^2\right]\int_0^b\int_0^a\sin\frac{m\pi x}{a}\sin\frac{n\pi y}{b}\phi_i(x)\,\varphi_j(y)\,\mathrm{d}x\mathrm{d}y\right\} \end{aligned} \tag{36}$$

At the same time the left side of Eq. (34) can also be simplified

$$D\sum_{m=1}^{M}\sum_{n=1}^{N}B_{mn}\left\{\begin{aligned}&\int_0^b\int_0^a\phi_m''(x)\,\varphi_n(y)\phi_i''(x)\,\varphi_j(y)\,\mathrm{d}x\mathrm{d}y+\int_0^b\int_0^a\phi_m(x)\varphi_n''(y)\,\phi_i(x)\,\varphi_j''(y)\,\mathrm{d}x\mathrm{d}y\\&+\upsilon\int_0^b\int_0^a\phi_m(x)\,\varphi_n''(y)\,\phi_i''(x)\,\varphi_j(y)\,\mathrm{d}x\mathrm{d}y+\upsilon\int_0^b\int_0^a\phi_m''(x)\,\varphi_n(y)\,\phi_i(x)\,\varphi_j''(y)\,\mathrm{d}x\mathrm{d}y\\&+2(1-\upsilon)\int_0^b\int_0^a\phi_m'(x)\,\varphi_n'(y)\,\phi_i'(x)\,\varphi_j'(y)\,\mathrm{d}x\mathrm{d}y\end{aligned}\right\} \tag{37}$$

Then the $M\times N$ equations of variable B_{mn} can be written as matrix form

$$\begin{bmatrix}\Phi_{11}^{11}&\Phi_{12}^{11}&\cdots&\Phi_{mn}^{11}&\cdots&\Phi_{MN}^{11}\\\Phi_{11}^{12}&\Phi_{12}^{12}&\cdots&\Phi_{mn}^{12}&\cdots&\Phi_{MN}^{12}\\\vdots&\vdots&\ddots&\vdots&\ddots&\vdots\\\Phi_{11}^{ij}&\Phi_{12}^{ij}&\cdots&\Phi_{mn}^{ij}&\cdots&\Phi_{MN}^{ij}\\\vdots&\vdots&\vdots&\vdots&\vdots&\vdots\\\Phi_{11}^{MN}&\Phi_{12}^{MN}&\cdots&\Phi_{mn}^{MN}&\cdots&\Phi_{MN}^{MN}\end{bmatrix}\begin{Bmatrix}B_{11}\\B_{12}\\\vdots\\B_{mn}\\\vdots\\B_{MN}\end{Bmatrix}=(1+\upsilon)a_T\,\frac{1}{2\lambda}\left\{1-\frac{96}{\pi^4}\sum_{n=1,3,5}^{\infty}\frac{e^{-n^2\beta t}}{n^4}\right\}\begin{Bmatrix}\Lambda_{11}\\\Lambda_{12}\\\vdots\\\Lambda_{ij}\\\vdots\\\Lambda_{MN}\end{Bmatrix} \tag{38}$$

where

$$\begin{aligned}\Phi_{mn}^{ij} =\ &\int_0^b\int_0^a\phi_m''(x)\,\varphi_n(y)\,\phi_i''(x)\,\varphi_j(y)\,\mathrm{d}x\mathrm{d}y+\int_0^b\int_0^a\phi_m(x)\,\varphi_n''(y)\,\phi_i(x)\,\varphi_j''(y)\,\mathrm{d}x\mathrm{d}y\\&+\upsilon\int_0^b\int_0^a\phi_m(x)\,\varphi_n''(y)\,\phi_i''(x)\,\varphi_j(y)\,\mathrm{d}x\mathrm{d}y+\upsilon\int_0^b\int_0^a\phi_m''(x)\,\varphi_n(y)\,\phi_i(x)\,\varphi_j''(y)\,\mathrm{d}x\mathrm{d}y\\&+2(1-\upsilon)\int_0^b\int_0^a\phi_m'(x)\,\varphi_n'(y)\,\phi_i'(x)\,\varphi_j'(y)\,\mathrm{d}x\mathrm{d}y\end{aligned} \tag{39}$$

$$\Lambda_{ij} = \sum_{m=1,3,5}^{\infty}\sum_{n=1,3,5}^{\infty}\left\{\frac{16q_T}{\pi^2 mn}\left[\left(\frac{m\pi}{a}\right)^2+\left(\frac{n\pi}{b}\right)^2\right]\int_0^a\sin\frac{m\pi x}{a}\phi_i(x)\,\mathrm{d}x\int_0^b\sin\frac{n\pi y}{b}\varphi_j(y)\,\mathrm{d}y\right\} \tag{40}$$

Substituting $B_{mn}(t) = (1+\upsilon)_T\,\frac{1}{2\lambda}\left\{1-\frac{96}{\pi^4}\sum_{n=1,3,5}^{\infty}\frac{e^{-n^2\beta t}}{n^4}\right\}\tilde{B}_{mn}$ into Eq. (38), each $\tilde{B}_{mn}$ can be obtained. So the quasi-static solution can be expressed as follows

https://doi.org/10.1017/jmech.2016.19 Published online by Cambridge University Press

$$w_s = \sum_{m=1}^{M}\sum_{n=1}^{N}\frac{(1+\upsilon)a_T}{2\lambda}\left\{1-\frac{96}{\pi^4}\sum_{n=1,3,5}^{\infty}\frac{e^{-n^2\beta t}}{n^4}\right\}\tilde{B}_{mn}\,\phi_m(x)\,\varphi_n(y) \tag{41}$$

3.4 Dynamic Solution for Rub-Impact Plate Under Thermal Shock

The deformations w_m is expanded by using the expression

$$w_m(x,\,y,\,t) = \sum_{i=1}^{I}\sum_{j=1}^{J} Q_{ij}(t)\cdot W_{ij}(x,\,y) \tag{42}$$

Substituting Eq. (42) into Eq. (19), we can get the expression though integral along the whole plate based on the orthogonality of vibration mode as follows

$$\ddot{Q}_{ij}(t) + \omega_{ij}^2 Q_{ij} = \frac{\int_0^b\int_0^a q'(x,\,y,\,t)\,W_{ij}(x,\,y)\,\mathrm{d}x\mathrm{d}y}{\int_0^b\int_0^a \rho h W_{ij}^2(x,\,y)\,\mathrm{d}x\mathrm{d}y} = \frac{\tilde{P}_{ij}(t)}{\tilde{M}_{ij}(t)} \tag{43}$$

where

$$q'(x,\,y,\,t) = q(x,\,y,\,t) + \rho h w_s\Omega^2 - \rho h\ddot{w}_s - \rho h\Omega^2(R+x)\frac{\partial w_s}{\partial x} + \rho h\Omega^2\left[R(a-x)+\frac{1}{2}(a^2-x^2)\right]\frac{\partial^2 w_s}{\partial x^2} \tag{44}$$

According to the single degree of freedom vibration theory, the solution of Eq. (43) can be obtained

$$Q_{ij}(t) = a_{ij}\sin\omega_{ij}\,t + b_{ij}\cos\omega_{ij}\,t + \frac{1}{\tilde{M}_{ij}\,\omega_{ij}}\int_0^t \tilde{P}_{ij}(\tau)\sin\omega_{ij}(t-\tau)\,\mathrm{d}\tau \tag{45}$$

where

$$\begin{aligned}\tilde{P}_{ij}(\tau) = {} & \int_0^b\int_0^a q(x,\,y,\,\tau)W_{ij}(x,\,y)\,\mathrm{d}x\mathrm{d}y + \rho h\Omega^2\frac{(1+\upsilon)a_T}{2\lambda}\left\{1-\frac{96}{\pi^4}\sum_{n=1,3,5}^{\infty}\frac{e^{-n^2\beta\tau}}{n^4}\right\}\int_0^b\int_0^a \Psi(x,\,y)\,W_{ij}(x,\,y)\,\mathrm{d}x\mathrm{d}y \\ & - \rho h\frac{\mathrm{d}^2}{\mathrm{d}\tau^2}\left[\frac{(1+\upsilon)a_T}{2\lambda}\left\{1-\frac{96}{\pi^4}\sum_{n=1,3,5}^{\infty}\frac{e^{-n^2\beta\tau}}{n^4}\right\}\right]\int_0^b\int_0^a \Upsilon(x,\,y)\,W_{ij}(x,\,y)\,\mathrm{d}x\mathrm{d}y\end{aligned} \tag{46}$$

$$\int_0^b\int_0^a \Psi(x,\,y)\,W_{ij}(x,\,y)\,\mathrm{d}x\mathrm{d}y = \int_0^b\int_0^a \left\{\begin{aligned}&\sum_{m=1}^{M}\sum_{n=1}^{N}\tilde{B}_{mn}\,\phi_m(x)\,\varphi_n(y) - (R+x)\sum_{m=1}^{M}\sum_{n=1}^{N}\tilde{B}_{mn}\,\dot{\phi}_m(x)\,\varphi_n(y) \\ &+\left[R(a-x)+\frac{1}{2}(a^2-x^2)\right]\sum_{m=1}^{M}\sum_{n=1}^{N}\tilde{B}_{mn}\,\ddot{\phi}_m(x)\,\varphi_n(y)\end{aligned}\right\}\sum_{ki=1}^{I}\sum_{kj=1}^{J}A_{kikj}^{ij}\,\phi_{ki}(x)\,\varphi_{kj}(y)\,\mathrm{d}x\mathrm{d}y \tag{47}$$

$$\int_0^b\int_0^a \Upsilon(x,\,y)\,W_{ij}(x,\,y)\,\mathrm{d}x\mathrm{d}y = \int_0^b\int_0^a \sum_{m=1}^{M}\sum_{n=1}^{N}\tilde{B}_{mn}\,\phi_m(x)\,\varphi_n(y)\sum_{ki=1}^{I}\sum_{kj=1}^{J}A_{kikj}^{ij}\,\phi_{ki}(x)\,\varphi_{kj}(y)\,\mathrm{d}x\mathrm{d}y \tag{48}$$

Equation (46) consists of rubbing load part and temperature load part. Substituting Eq. (45) into Eq. (42), forced response without the initial vibration can be expressed as follows

$$w_m(x,\,y,\,t) = \sum_{i=1}^{I}\sum_{j=1}^{J}\left[D_{ij}^{(1)}(t) + D_{ij}^{(2)}(t)\right] \tag{49}$$

where

$$D_{ij}^{(1)}(t) = \frac{\mu\int_0^b F_{\max}(y)\,W_{ij}(a,\,y)\,\mathrm{d}y}{\tilde{M}_{ij}}\cdot W_{ij}(x,\,y)\left\{\frac{a_0'}{\omega_{ij}^2} + \sum_{k=1}^{\infty}\left[\frac{a_k'}{\omega_{ij}^2-\omega_d^2}\cos(\omega_d t) + \frac{b_k'}{\omega_{ij}^2-\omega_d^2}\sin(\omega_d t)\right]\right\} \tag{50}$$

https://doi.org/10.1017/jmech.2016.19 Published online by Cambridge University Press

$$D_{ij}^{(2)}(t)=\frac{W_{ij}(x,y)}{\tilde{M}_{ij}\,\omega_{ij}}\left\{\begin{array}{l}\left[\rho h\Omega^2\dfrac{(1+\upsilon)a_T}{2\lambda}\iint_s \Psi(x,y)\,W_{ij}(x,y)\,\mathrm{d}s\right]\cdot\int_0^t\left\{1-\dfrac{96}{\pi^4}\sum_{n=1,3,5}^{\infty}\dfrac{e^{-n^2\beta\tau}}{n^4}\right\}\sin\omega_{ij}(t-\tau)\,\mathrm{d}\tau\\ -\left[\rho h\iint_s \Upsilon(x,y)\,W_{ij}(x,y)\,\mathrm{d}s\right]\cdot\int_0^t\dfrac{\mathrm{d}^2}{\mathrm{d}\tau^2}\left[\dfrac{(1+\upsilon)a_T}{2\lambda}\left\{1-\dfrac{96}{\pi^4}\sum_{n=1,3,5}^{\infty}\dfrac{e^{-n^2\beta\tau}}{n^4}\right\}\right]\sin\omega_{ij}(t-\tau)\,\mathrm{d}\tau\end{array}\right\} \tag{51}$$

where $\omega_d=2k\pi/T_c$, $a_0'=a_0/F_{\max}(y)$, $a_k'=a_k/F_{\max}(y)$, $b_0'=b_0/F_{\max}(y)$. From what has been discussed above, we can find that the final vibration response consists of the vibration response caused by rubbing and the vibration response under thermal shock.

4. RESULTS AND DISCUSSION

4.1 Modal Characteristic Analysis

In the following work, beam mode functions are employed for $M=N=7$ to generate 49 plate mode functions. To compare the numerical results with those in the work by Yoo [21] and check the convergence of the lowest five natural frequencies, dimensionless parameters are set as $\chi=a/b=1$, $\lambda=R/a=1$, $\gamma=\Omega/\sqrt{\rho h a^4/D}=1$

As shown in Fig. 4, the internal convergence is investigated in the case of different assumed mode functions ($M=N$). It can be observed from the figure that the maximal relative error is less than 0.4% and curves tend to be steady, which indicates the sufficient convergence.

Table 1 compares the lowest five natural frequencies in the case of $M=N=7$ and existing results. A great precision can be found in the case of assumed modes number $M=N=7$ and 49 mode functions are accurate to obtain the results in this study. On the other hand the first three order bending vibration modes of the rotating cantilever plate are shown as follows

4.2. Rub-Induced Vibration in Different Locations

In this section, we concentrate on the effects of different locations on the rub-induced vibration. It is assumed that $F_{\max}=6400\mathrm{N}$, $\Omega=300\mathrm{rad/s}$, $\mu=0.3$, $a=100\mathrm{cm}$, $b=30\mathrm{cm}$, $q_T=0$. And the other general parameters are shown in Table 2.

Now the analytical solution is used to analyze the vibration behavior of the rotating plate. As shown in Fig. 6(a), dynamic response curves at three different locations for $x=a$ are different distinctly. On the other hand it can be seen that rubbing appears at $t=t_p/2$ from Fig. 6(b). Vibration mode shows complex vibration and the difference of rub-induced vibration of plate corner point in width direction is obvious. So one-dimensional beam model cannot describe the rubbing dynamic behavior and it is more accurate to simplify as two-dimensional plate model.

Figure 7 gives the dynamic responses of rotating cantilever plate for $(\xi,\ \eta)=(a,\ b/4)$. Although the difference of rub-induced vibrations still exists, it decreases gradually compared with the vibrations of plate corner point.

Table 1 Comparison of the lowest five dimensionless natural frequencies.

Mode	1	2	3	4	5
Yoo Method	3.7324	8.6240	21.706	27.394	31.350
$M=N=7$	3.7317	8.6214	21.702	27.358	31.340
Error (%)	0.019	0.030	0.018	0.131	0.032

Table 2 Parameters used for the analysis.

E (GPa)	υ	ρ (kg/m^3)	h (mm)	R (cm)	T_c	t_p
117	0.3	4466	7.47	50	$2\pi/\Omega$	$0.01T_c$

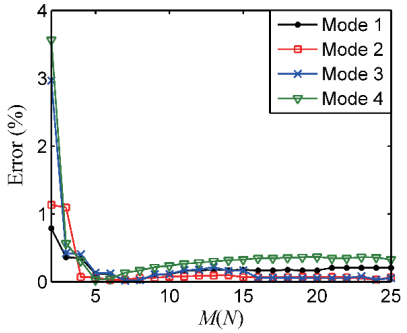


Fig. 4 Convergence of the natural frequencies in the case of different assumed mode functions.

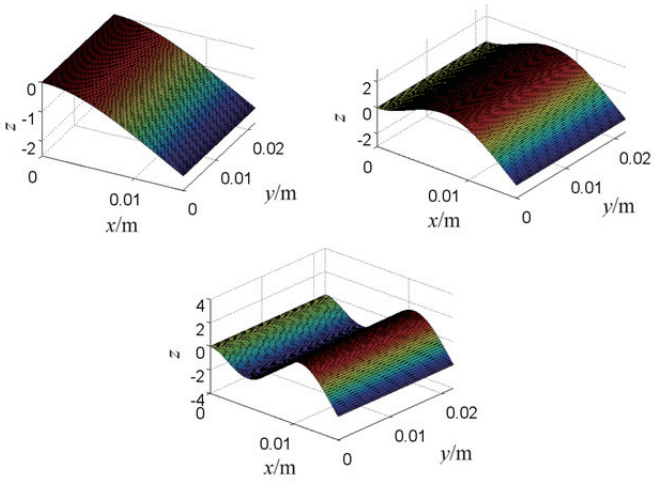
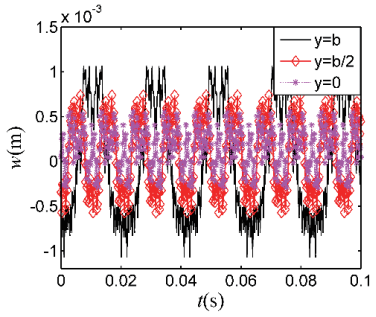
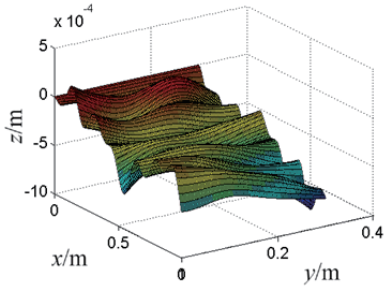


Fig. 5 First three modes of rotating cantilever plate at $M=N=7$.

https://doi.org/10.1017/jmech.2016.19 Published online by Cambridge University Press

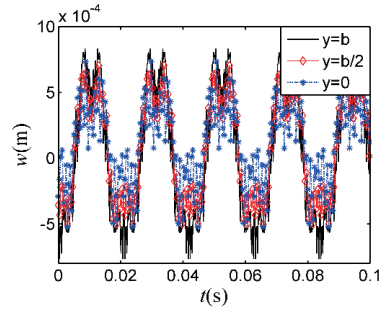


(a) Response curves at different locations for $x = a$

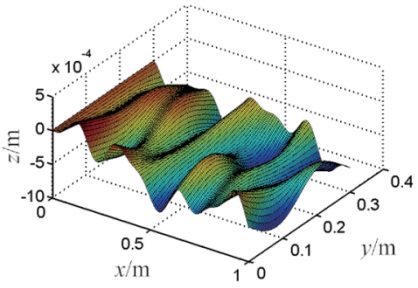


(b) Vibration mode at $t = t_p / 2$

Fig. 6 Dynamic responses of rotating cantilever plate for $(\xi, \eta) = (a, 0)$.



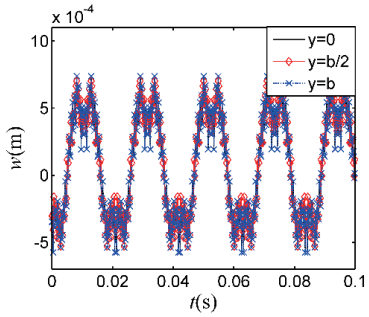
(a) Response curves at different locations for $x = a$



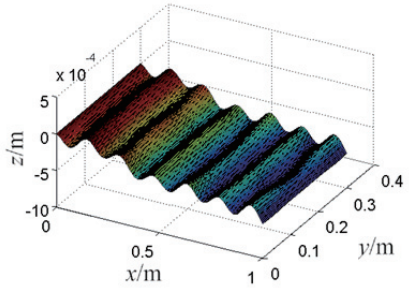
(b) Vibration mode at $t = t_p / 2$

Fig. 7 Dynamic responses of rotating cantilever plate for $(\xi, \eta) = (a, b/4)$.

When the rubbing point change to $(a, b/2)$, dynamic response curves at three different locations are in good agreement. It can be seen clearly from Fig. 8 that the rub-induced vibration in width direction are consistent relatively. At this time one-dimensional beam model can instead of two-dimensional model. But with the increase of rotation speed ω, the conclusion is no longer true.



(a) Response curves at different locations for $x = a$



(b) Vibration mode at $t = t_p / 2$

Fig. 8 Dynamic responses of rotating cantilever plate for $(\xi, \eta) = (a, b/2)$.

4.3 Influence of the Rotation Speeds on Tip-Rub

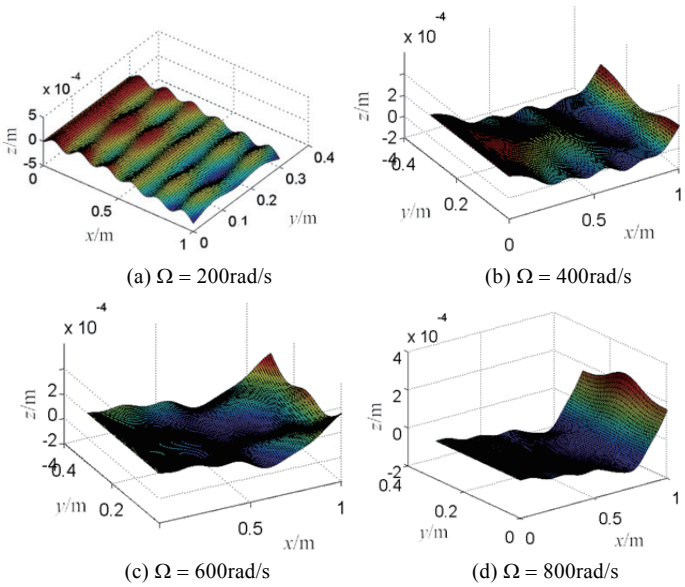
In this section, we consider the influence of different rotation speeds on rotating plate. It can be found from Figs. 9(a) to 9(b) that vibration of the plate in width direction is different. The symmetry of vibration under low rotation speed is destroyed with the increase of rotation speed ω. Vibration displacements mutate gradually among 0.76m and 1m and is several times even dozens of times larger than the rest parts. Because the rubbing force and amplitude are large relatively and action time is short, other parts of the plate have not changed in time. At the same time, as the action of rubbing force, the torsional fracture failure easily occurred.

As shown in Fig. 10, the vibration amplitude and phase of each location at the edge are approximate sine pulse waves and all different. So one-dimensional beam model is no longer applicable in the case of high rotation speed. From what has been discussed above, it is more accurate to use two-dimensional plate model than one-dimensional beam model when describing the dynamic response of rubbing rotating blade.

4.4 Discussion of the Rubbing Force Form

Figure 11 shows vibration modes of rotating cantilever plate for $F_{max}(y) = 6400$N. It can be observed that vibration of the plate in width direction is consistent at low rotation speed. In combination with Fig. 12, vibration amplitude at $y = 0$ is smaller than that in other places when $\Omega = 800$rad/s. There is a certain difference in rubbing vibration amplitude and the change is small. So line rubbing with constant $F_{max}(y)$ can be described approximately using one-dimensional beam model. But there is definite error. To compare Figs. 11(a) with 11(b), it can be found that line rubbing and point rubbing have similar characteristics with the increase of rotation speed ω.

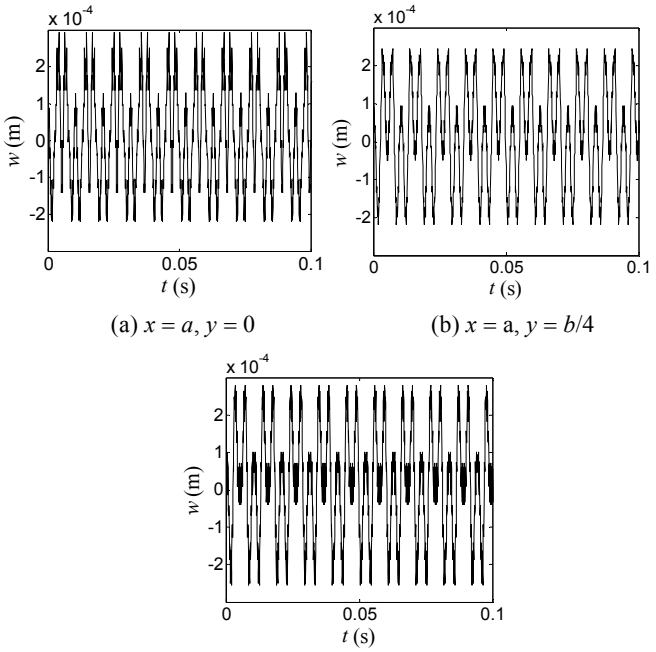
https://doi.org/10.1017/jmech.2016.19 Published online by Cambridge University Press



(a) Ω = 200rad/s (b) Ω = 400rad/s

(c) Ω = 600rad/s (d) Ω = 800rad/s

Fig. 9 The influence of rotation speed on rotating cantilever plate for $(\xi, \eta) = (a, b/2)$, $t = t_p / 2$.

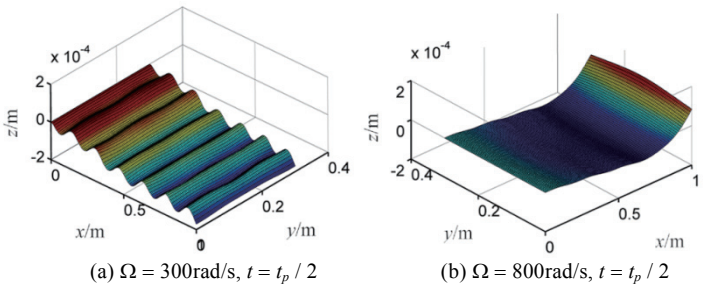


(a) $x = a$, $y = 0$ (b) x = a, $y = b/4$

(c) $x = a$, $y = b/2$

Fig. 10 Time history curves of rotating cantilever plate at different positions for ω = 600rad/s.

In general case, the amplitude of rubbing force in width direction is not equal. It is assumed that $F_{\max}(y)$ $F_{\max}(y) = y(f_2 - f_1)/b + f_1$ with $f_1 = 6400$N, $f_2 = 0$. The difference of vibration in width direction is as shown in Fig. 13(a). When the rotation speed comes to 800rad/s, the phenomenon that vibration displacements change gradually along width direction appears. At the same time Fig. 14 shows that the amplitudes and phases at $y = 0.35b$ and $y = 0.76b$ are different. So we can come to a conclusion that line rubbing needs to be described with plate model and one-dimensional beam model is no longer applicable.



(a) Ω = 300rad/s, $t = t_p / 2$ (b) Ω = 800rad/s, $t = t_p / 2$

Fig. 11 Dynamic responses of rotating cantilever plate with constant rubbing for $F_{\max}(y) = 6400$N.

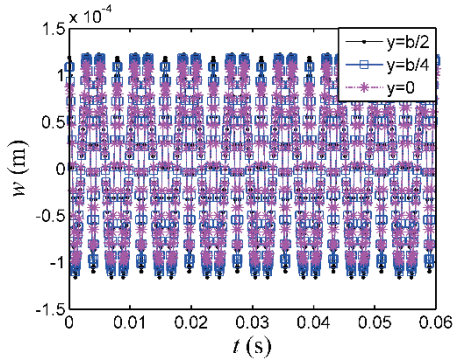
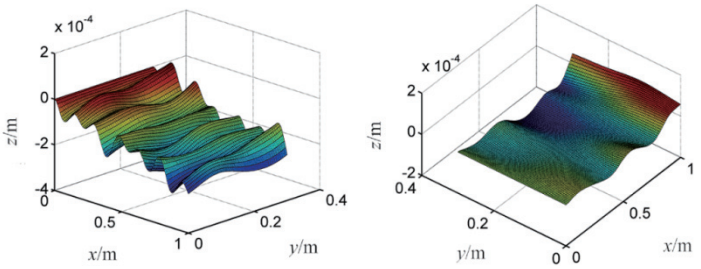


Fig. 12 Response curves at different locations with linear rubbing for $x = a$, $F_{\max}(y) = 6400$N, Ω = 800rad/s.



(a) Ω = 300rad/s, $t = t_p / 2$ (b) Ω = 800rad/s, $t = t_p / 2$

Fig. 13 Dynamic responses of rotating plate with linear rubbing when $F_{\max}(y)$ to be linear function.

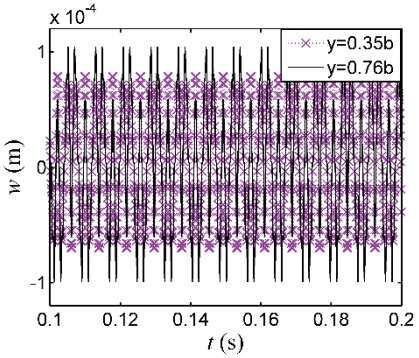


Fig. 14 Response curves at different locations with linear rubbing when $F_{\max}(y)$ to be linear function: $x = a$, Ω = 800rad/s.

https://doi.org/10.1017/jmech.2016.19 Published online by Cambridge University Press

4.5 Study on Thermal Shock

In practice, a rubbing blade from high-pressure compressor is often accompanied by the thermal shock problem. In order to investigate the influence of thermal shock on rub-induced vibrations, the following results are shown in Figs. 15 ~ 19. The parameters are considered as $a = b = 30$cm, $F_1 = 1000$N, $F_2 = 2000$N, $a_T = 17.8 \times 10^{-6}$K^{-1}, $\lambda = 50$W/(m·K), $c = 500$J/(kg·K), $\Omega = 300$rad/s, $\mu = 0.2$. There is only rubbing fault when $q_T = 0$W/m^2. As shown in Fig. 15, the nonuniformity of rubbing force along the edge caused the difference of vibration in width direction.

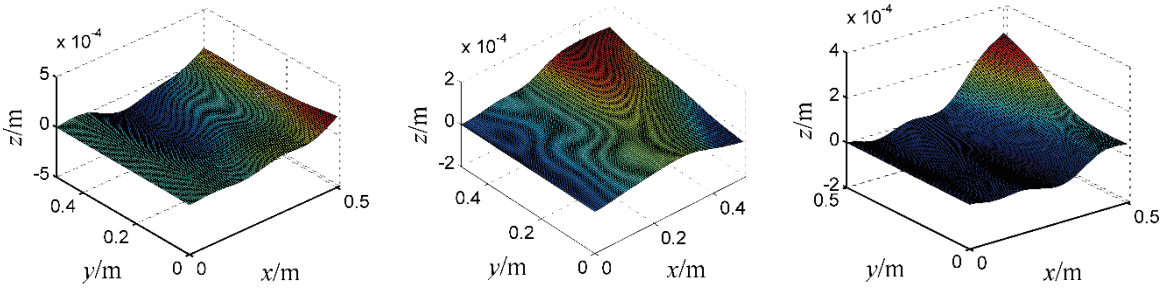
When thermal shock increases to 200W/m^2, it can be found that the increase of thermal flow q_T leads to an increase of the thermal shock vibration and a decrease of the difference of vibration in width direction. This phenomenon is intensified by the larger thermal flow q_T as shown in Fig. 17. That is to say the effect of thermal shock makes consistent vibration of rotating plate in width direction. And vibration displacement increases gradually away from fixed support. This phenomenon is different from the effects of rubbing fault. Compared with thermal shock failure, uneven rubbing is more likely to lead to torsion fracture.

The time responses for $x = a$, $y = b/4$ with different thermal flow are shown in Fig. 18. With the increase of thermal flow, multiperiodicity and complexity of vibration are reduced. But it can lead to the rapid increase of vibration amplitude. Thermal shock vibration need to be avoided in practical engineering.

Figure 19 gives the corresponding frequency spectrums in Fig. 18. There are many vibration frequency components caused by rubbing fault without thermal shock and the high frequency vibration is significant in Fig. 19(a). After applied thermal shock, namely, thermal flow comes to 100W/m^2, vibration frequency components and the contribution of high frequency vibration reduce, low frequency vibration aggravates as shown in Fig. 19(c). With the increase of thermal flow, vibration frequency components continue to reduce. When thermal flow increases to 500W/m^2, rubbing vibration is presented as low frequency vibration. So we can come to a conclusion that thermal shock vibration manifests as simple low frequency vibration. On the contrary rubbing vibration manifests as complicated multiple frequency coupling vibration. The increase of thermal flow reduces high frequency vibration and aggravates the vibration of plate. Thus, this phenomenon is also need to be avoided.

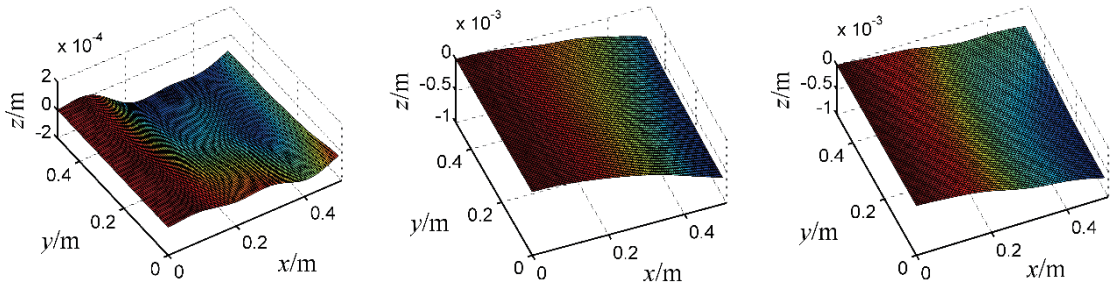
4.6 The Effects of Friction Coefficient

Considering the results in Figs. 20 and 21 when $q_T = 200$W/m^2, we discuss vibration and the frequency of the rotating plate with different friction coefficient μ. Giving responses with the friction coefficient $\mu = 0.05$, 0.1, 0.3, Fig. 20 indicates that vibration amplitude increases gradually and the complexity of vibration aggravates with the increase of friction coefficient. In addition, high frequency vibration is more significant as shown in Fig. 21. The above results indicate that the increase of the friction coefficient leads to an increase in rubbing fault. In fact, the decreasing friction coefficient uniquely decreases the friction force μF_n, which shows the friction effect is an important factor to trigger the rubbing phenomenon. Reducing the surface roughness can be used in the process of practical work.



(a) $t = 50T_c + 0.5t_p$ (b) $t = 50T_c + 15t_p$ (c) $t = 50T_c + 20t_p$

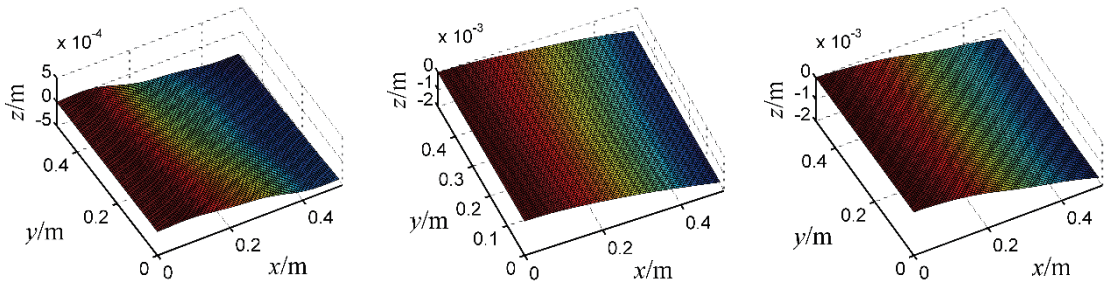
Fig. 15 Vibration modes of the rubbing plate with $q_T = 0$W/m^2 at different times.



(a) $t = 50T_c + 0.5t_p$ (b) $t = 50T_c + 15t_p$ (c) $t = 50T_c + 20t_p$

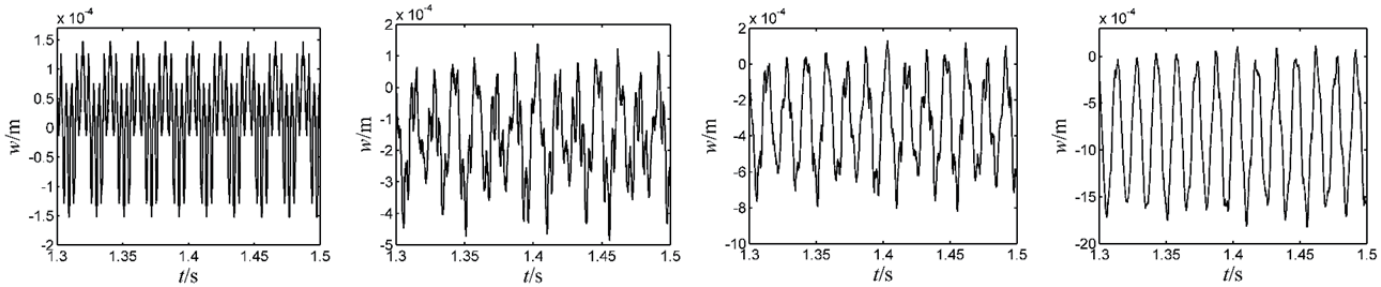
Fig. 16 Vibration modes of the rubbing plate with $q_T = 200$W/m^2 at different times.

https://doi.org/10.1017/jmech.2016.19 Published online by Cambridge University Press



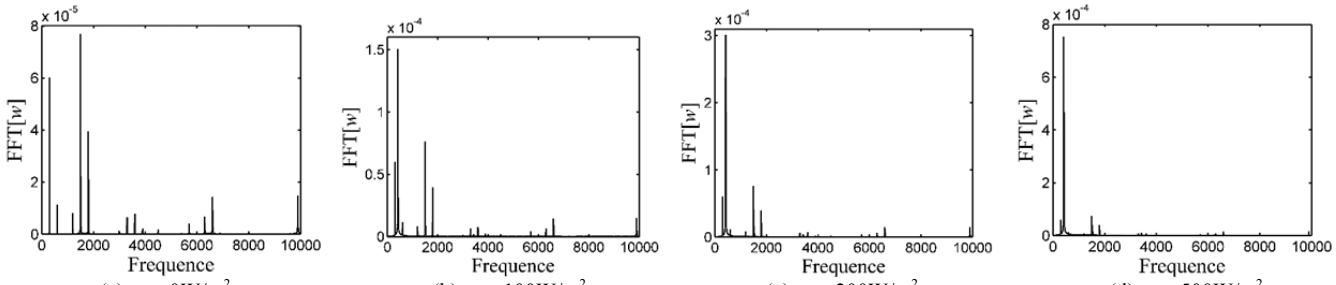
(a) $t = 50T_c + 0.5t_p$ (b) $t = 50T_c + 15t_p$ (c) $t = 50T_c + 20t_p$

Fig. 17 Vibration modes of the rubbing plate with q_T= 500W/m^2 at different times.



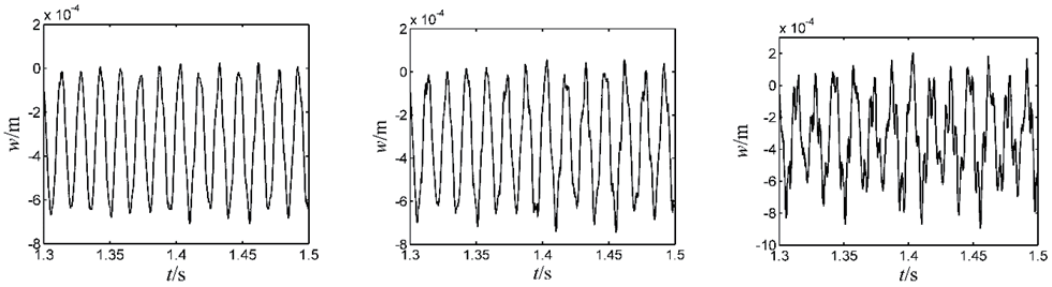
(a) q_T= 0W/m^2 (b) q_T= 100W/m^2 (c) q_T= 200W/m^2 (d) q_T= 500W/m^2

Fig. 18 Time responses of the rubbing plate for different thermal flow q_T.



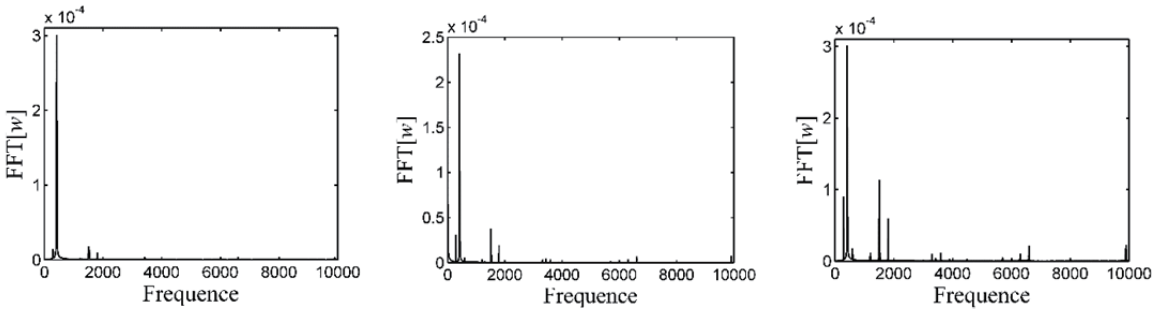
(a) q_T= 0W/m^2 (b) q_T= 100W/m^2 (c) q_T= 200W/m^2 (d) q_T= 500W/m^2

Fig. 19 Frequency spectrums of the rubbing plate for different thermal flow q_T.



(a) $\mu = 0.05$ (b) $\mu = 0.1$ (c) $\mu = 0.3$

Fig. 20 Time responses of the rubbing plate for different thermal flow q_T.



(a) $\mu = 0.05$ (b) $\mu = 0.1$ (c) $\mu = 0.3$

Fig. 21 Frequency spectrums of the rubbing plate for different thermal flow q_T.

https://doi.org/10.1017/jmech.2016.19 Published online by Cambridge University Press

5. CONCLUSIONS

In the present paper, a contact-impact model is developed for rub-induced vibrations of a rotating plate under thermal shock. Analytical solution is carried out to study on the present contact model. The variability of deformations in width direction demonstrates plate models can be accurate and reliable for vibration analysis of constant aspect ratio blades. Then the dynamic responses of rub-induced vibrations and the influence of the locations, rotation speeds, rubbing force form, thermal shock and friction coefficients are investigated.

The results indicate that with the increase of rotation speed, rubbing force time change shorter, the amplitude of rubbing force near the free end is larger, mutations of vibration intensity is easy to cause torsion fracture failure. On the other hand more thermal flow aggravates thermal shock vibration, weaken the difference in width direction caused by rubbing force and make plate be low frequency vibration. Moreover, the increasing friction coefficient and friction force enhance rub-induced vibrations.

ACKNOWLEDGEMENTS

National Science Foundation of China (Grant No. 51275081); Major Project of National Science Foundation of China (Grant No. 51335003).

REFERENCES

1. Muszynska, A., "Rotor to Stationary Element Rub-Related Vibration Phenomena in Rotating Machinery," *Shock and Vibration*, **21**, pp. 3–11(1989).
2. K.Choy, F. and Padovan, J., "Nonlinear Transient Analysis of Rotor-Casing Rub Events," *Journal of Sound and Vibration*, **113**, pp. 529–545 (1987).
3. Yao, M. H., Chen, Y. P. and Zhang, W., "Nonlinear Vibrations of Blade with Varying Rotating Speed," *Nonlinear Dynamics*, **68**, pp. 487–504 (2012).
4. Yoo, H. H. and Kim, S. K., "Flapwise Bending Vibration of Rotating Plates," *International Journal for Numerical Methods in Engineering*, **55**, pp. 785–802 (2002).
5. Legrand, M., Batailly, A., Magnain, B., Cartraud, P. and Pierre, C., "Full Three-Dimensional Investigation of Structural Contact Interactions in Turbo Machines," *Journal of Sound and Vibration*, **331**, pp. 2578–2601 (2012).
6. Batailly, A., Legrand, M., Millecamps, A. and Garcin, F., "Numerical-Experimental Comparison in the Simulation of Rotor/Stator Interaction Through Blade-Tip/Abradable Coating Contact," *Journal of Engineering for Gas Turbines and Power*, **134**, p. 082504 (2012).
7. Jiang, J., Ahrens, J. and Ulbrich, H., "A Contact Model of a Rotating Rubbing Blade. Proceedings of the 5th International Conference on Rotor Dynamics," *Darmstadt: International Federation for the Promotion of Mechanism and Machine Science Main*, pp. 478–489 (1998).
8. Young, G., "Development of a General Predictive Model for Blade Tip/Shroud Interference; Interactive Forces," Ph.D. Dissertation, the Ohio State University, Ohio, U.S. (2006).
9. Garza, J. W., "Tip Rub Induced Blade Vibrations: Experimental and Computational Results," Ph.D. Dissertation, the Ohio State University, Ohio, U.S. (2006).
10. Ferguson, J. L., "A Moving Load Finite Element-Based Approach to Determining Blade Tip Forces During a Blade-on-Casing Incursion in a Gas Turbine Engine," Ph.D. Dissertation, the Ohio State University, Ohio, U.S. (2008).
11. Millecamps, A., Brunel, J. F., Dufrenoy, P., Garcin, F. and Nucci, M., "Influence of Thermal Effects During Blade-Casing Contact Experiments," *ASME 2009 International Design Engineering Technical Conferences and Computers and Information in Engineering Conference*, San Diego, California, U.S., pp. 855–862 (2009).
12. Padova, C., Barton, J., Dunn, M. G. and Manwaring, S., "Development of an Experimental Capability to Produce Controlled Blade Tip/Shroud Rubs at Engine Speed," *Journal of Turbomach*, **127**, pp. 726–735 (2005).
13. Padova, C., Barton, J., Dunn, M. G. and Manwaring, S., "Experimental Results From Controlled Blade Tip/Shroud Rubs at Engine Speed," *Journal of Turbomach*, **129**, pp. 713–723 (2007).
14. Sinha, S. K., "Non-Linear Dynamic Response of a Rotating Radial Timoshenko Beam with Periodic Pulse Loading at the Free-End," *International Journal of Non-Linear Mechanics*, **40**, pp. 113–149 (2005).
15. Sinha, S. K., "Combined Torsional-Bending-Axial Dynamics of a Twisted Rotating Cantilever Timoshenko Beam with Contact-Impact Loads," *Journal of Applied Mechanics*, **74**, pp. 505–522 (2007).
16. Lesaffre, N., Sinou, J. J. and Thouverez, F., "Contact Analysis of a Flexible Bladed-Rotor," *European Journal of Mechanics A—Solids*, **26**, pp. 541–557 (2007).
17. Lesaffre, N., Sinou, J. J. and Thouverez, F., "Stability Analysis of Rotating Beams Rubbing on an Elastic Circular Structure," *Journal of Sound and Vibration*, **299**, pp. 1005–1032 (2007).
18. Batailly, A., Legrand, M., Cartraud, P. and Pierre, C., "Assessment of Reduced Models for the Detection of Modal Interaction Through Rotor Stator Contacts," *Journal of Sound and Vibration*, **329**, pp. 5546–5562 (2010).
19. Pereira, T. R., Engelen, A. H. and Pearson, G. A., "Response of Kelps from Different Latitudes to

https://doi.org/10.1017/jmech.2016.19 Published online by Cambridge University Press

Consecutive Heat Shock," *Journal of Experimental Marine Biology and Ecology*, **463**, pp. 57–62 (2015).

20. Sadowski, T. and Nakonieczny, K., "Thermal Shock Response of FGM Cylindrical Plates with Various Grading Patterns," *Composite Mater Science*, **43**, pp. 171–178 (2008).
21. Hein, J., Storm, J. and Kuna, M., "Numerical Thermal Shock Analysis of Functionally Graded and Layered Materials," *International Journal of Thermal Sciences*, **60**, pp. 41–51 (2012).
22. Song, Z. G. and Li, F. M., "Aerothermoelastic Analysis of Nonlinear Composite Laminated Panel with Aerodynamic Heating in Hypersonic Flow," *Mechanical Mater*, **34**, pp. 135–144 (2014).
23. Yoo, H. H. and Pierre, C., "Modal Characteristic of a Rotating Rectangular Cantilever Plate," *Journal of Sound and Vibration*, **259**, pp. 81–96 (2003).

(Manuscript received April 10, 2015,
accepted for publication January 8, 2016.)

https://doi.org/10.1017/jmech.2016.19 Published online by Cambridge University Press